Iceland Liechtenstein Norway grants

Working together for a green, competitive and inclusive Europe

Executive Agency for Higher Education, Research, Development and Innovation Funding

Toward Large Area Perovskite Solar Cells

(PERLA-PV)

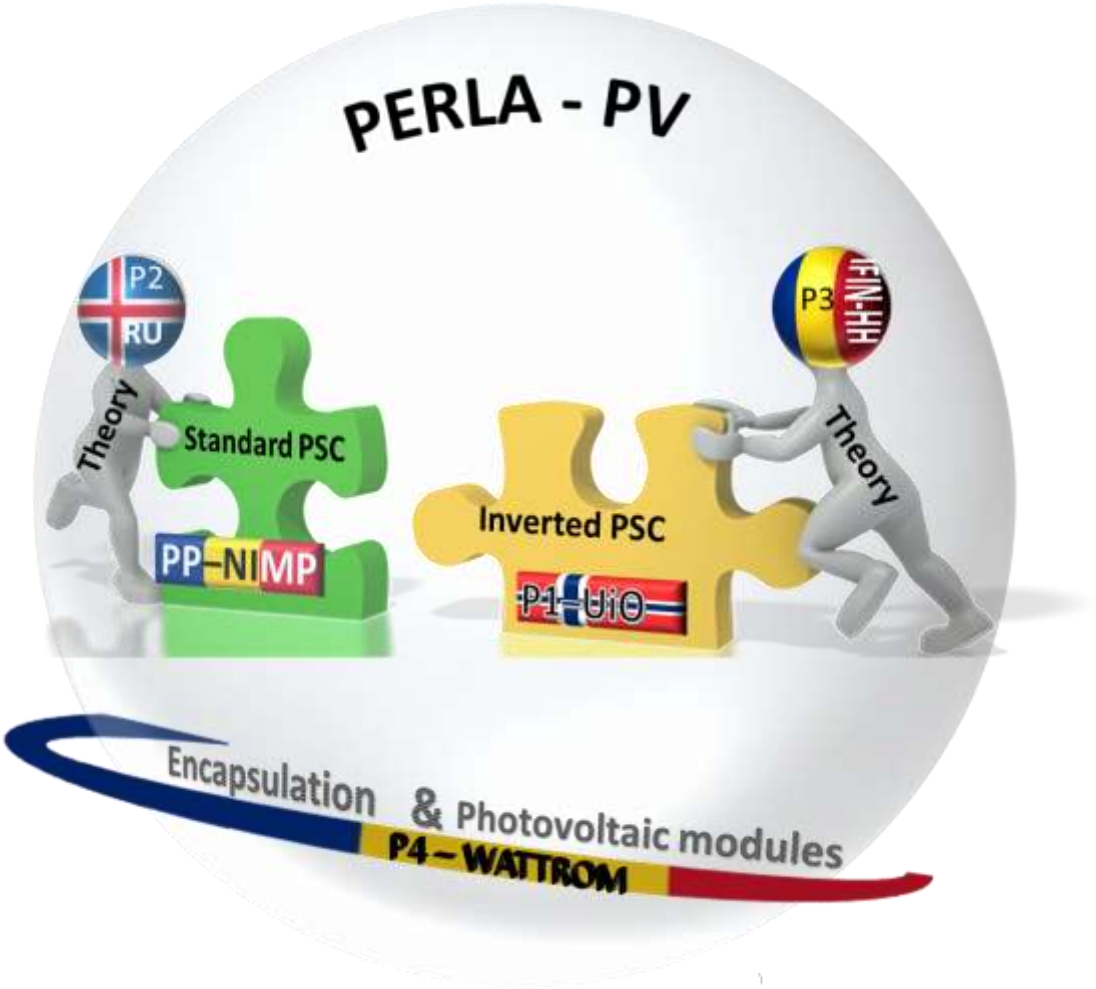

2021

The NEED for research in photovoltaics

Energy is the driving force behind the development of the human civilization, through technology and innovation. In the last century, the fossil fuel resources, as stored during hundreds of millions of years, are being rapidly depleted by excessive exploitation. The world population is estimated to stabilize around 10 billion up to 2050, leading to an energy demand that may significantly exceed the capabilities of conventional sources. A solution to this fast coming shortfall in energy is to take advantage of the renewable sources of energy available on Earth. Among them, the most abundant and clean, having the greatest potential of all is the solar energy. However, although in principle the Sun energy falling on Earth can cover the whole need of world's energy, only a very limited part of it is presently used by mankind. The main reasons are related to the costs and the knowledge of manufacturing efficient devices for energy conversion. A major challenge for the research community is to develop reasonable cheap, environmental friendly materials, devices and integrated photovoltaic systems converting the sunlight directly into electricity. The perovskite solar cells (PSC) have attracted a considerable interest in photovoltaics community, showing a very fast development in terms of power conversion efficiency (PCE), reaching now values above 25% certified PCE in not stabilized small area samples, proving that they can become real competitors to commonly used solar-cell materials (e.g Si). Not only the remarkably large PCE is an important asset, but also the low production costs makes the PSCs very attractive for the solar cell technology, as solution processing techniques are typically employed. In addition, they can be hosted by a long range of flexible substrates pushing further the record for power per weight and implicitly their utility. However, while the high PCE values and the expected low production costs are important advantages for PSCs, the real challenges to overcome prior to any attempt of industrial production are their *stability in time*, *reliability* and *reproducibility of the performance* as well as *environmental issues* raised by the use of toxic elements/solvents. These are well known problems for the small area standard and inverted PSCs, produced by spin-coating in research laboratories and inherently remain the same when envisaged is the fabrication of large area devices. *The project addresses these issues starting from the premise that coherent experimental and theoretical studies should be done using from the start cheap deposition techniques applicable on large areas (printing and sputtering).* Beside allowing the scaling up, such techniques can be better controlled offering a better homogeneity in deposition than the spin-coating method. The present project includes fundamental and applicative research aiming to achieve both scientific and practical goals. The **PERLA-PV** project addresses the development of efficient large area perovskite solar cells (PSC) and photovoltaic modules using cheap and environmental friendly technologies. Based on certified record values, as-grown (unstabilized) small area PSCs achieved a power conversion efficiencies over 25%, outperforming some types of Si solar cells, CdTe and CIGS cells. Being also inexpensive to produce, thin, light and suitable for fabrication with printing technologies the PSCs have in principle a great potential for large scale applications and commercialisation. However, prior to any attempt of industrial production, several challenges have to be overcome: enhance the reliability and reproducibility of PSCs, while reducing the toxicological and environmental issues raised by the use of toxic elements/solvents during the fabrication process. The consortium is composed by 5 partners: project promotor PP - National Institute of Materials Physics (NIMP), P3- *Horia Hulubei National Institute for R&D in Physics and Nuclear Engineering* (IFIN-HH) and P4 - Tritech Group (WATTROM), a SME as end-user, all from

Romania; P1- Oslo University (UiO) from Norway and P2 -Reykjavik University (RU) from Iceland.

Specific objectives to be achieved during the project are:

O1- understand the physical working principles of perovskite solar cells and find solutions to increase and stabilize the PCE while enlarging the area of the cells;

O2 – reduce the amount of costly materials and toxic solvents used in the fabrication process of both standard and inverted PSC structures with other inexpensive and environmental friendly

O3 - stabilize the PCE performance of PSC via compositional engineering and proper replacements including the selective contacts

O4 – enhance the charge collection efficiency by optimizing interfaces between the layers in the cell

O5 - develop cheap large area fabrication technologies (printing and sputtering) for all the component layers in PSCs, standard and inverted structures

O6 - obtain efficient large area encapsulated PSCs and photovoltaic modules with PCE over 15%

Research and results in 2021

Work carried out by the participants according to work packages (WP) in the project

WP1: Preparation of standard PSCs

PP (NIMP) has worked on:

- Install a suitable printing equipment in glow box (Fig. 1).

Figure 1. Slot-die system installed in glovebox during a deposition

- Deposition of the compact and mesoporous ETL layers by spray coating and characterization, As compact layer we used TiO_2. For the mesoporous layer we considered: TiO_2, SnO_2 and Quantum Dots of SnO_2 (QD-SnO_2). The deposited layers were investigated by XRD, AFM and SEM. In total, 108 samples have been prepared and characterized for finding the optimal deposition conditions (dilution, temperature and treatment time).

- Prepare, deposit and characterize the hole transporter layer (HTL), (1) *organic,* the commonly used SpiroOMeTAD and *(2) inorganic* based on Cu and Ni-doped Cu oxides deposited by reactive radio-frequency magnetron sputtering under different deposition conditions (see Table 1).

Table 1: RF-MS deposition conditions and corresponding sample codes.

Sample batch code	Total gas pressure (Pa)	Target–substrate distance (mm)	O_2 dilution (%) / O_2 partial pressure (Pa)	Ni racetrack addition (pcs)
A5.0	0.3	35	5 / 0.015	n/a
A7.5	0.3	35	7.5 / 0.0225	n/a
A10.0	0.3	35	10 / 0.3	n/a
2Ni:A7.5	0.3	35	7.5 / 0.0225	2
4Ni:A7.5	0.3	35	7.5 / 0.0225	4

Cu and Ni oxide films of ~2000, ~500 and ~100 nm were obtained. The deposited films were investigated by means of SEM (Fig. 2), ellipsometry, XPS, XRD, optical transmission, four-point resistivity and Hall measurements. The fitting of the XRD diagrams indicated that the crystal structure of each film can be modelled with a mixture of two Cu_2O phases.

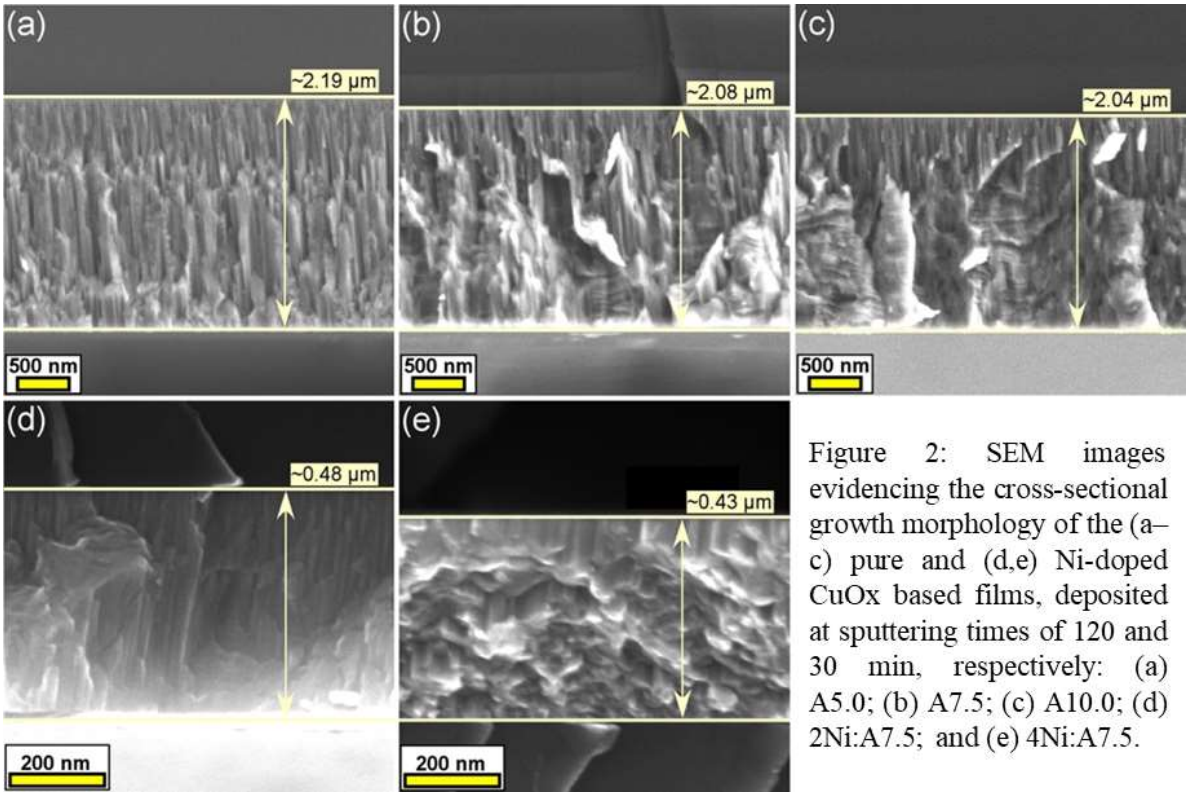

Figure 2: SEM images evidencing the cross-sectional growth morphology of the (a–c) pure and (d,e) Ni-doped CuOx based films, deposited at sputtering times of 120 and 30 min, respectively: (a) A5.0; (b) A7.5; (c) A10.0; (d) 2Ni:A7.5; and (e) 4Ni:A7.5.

According to XPS, the binding energy positions of both the Cu 2p and Ni 2p core electron levels unveiled their complete oxidation. The binding energy of the Ni $2p_{3/2}$ peak (~854.5 – 855.8 eV) indicated a higher oxidation state of Ni, characteristic to a Ni_2O_3 or a complex Cu-Ni oxide. The band gaps and Urbach energies of the as-sputtered pure and Ni-doped Cu_2O-based films are given in Table 2. The carrier density increased sharply, from 1.5×10^{14} to 2.6×10^{15} cm^{-3}, with the increase of the O ratio in the gas ambient up to 7.5 vol. %. Hall

measurements have shown that the pure p-type Cu_2O based layers have a remarkable high carrier's mobility, up to ~1200 cm^2/Vs (for p-type A5.0).

Sample code	E_g (eV)	E_U (meV)
A5.0	2.50	235
A7.5	2.55	271
A10.0	2.61	301
2Ni:A7.5	2.68	308

Table 2: *Band gaps and Urbach energies of the as-sputtered pure and Ni-doped Cu_2O-based thin films.*

- Prepare, deposit and characterize compositional and solvent engineered HP absorbers, starting from the $CH_3NH_3PbI_3$ (MAPI) to compositional engineered HP double perovskites: $CH_3NH_3PbI_{2.6}Cl_{0.4}$; $CH_3NH_3PbI_{1.8}Br_{1.2}$; $CH_3NH_3PbI_{1.8}Cl_{1.2}$; $(CH_3NH_3)_{1-x}(C_3N_2H_5)_xPbI_{2.6}Cl_{0.4}$ with x from 0 to 1; $(HC(NH_2)_2)_{0.7}(CH_3NH_3)_{0.2}PbI_{2.8}Cl_{0.2}$; $K_{0.1}FA_{0.7}MA_{0.2}PbI_{2.8}Cl_{0.2}$, $FA_{0.8}MA_{0.2}PbI_{2.8}Cl_{0.2}$, $K_{0.1}FA_{0.8}MA_{0.2}PbI_{2.8}Cl_{0.2}/CsPbBr_3$ and $K_{0.1}FA_{0.8}MA_{0.2}PbI_{2.8}Cl_{0.2}/CsPb_2Br_5$. Characterization by XRD, SEM, AFM. The solvent engineering had focused on: (i) *Anti-solvent engineering of the on $FA_{0.8}MA_{0.2}Pb\ I_{2.8}Cl_{0.2}$* (FAMA) with the aim of evaluating, the benefit of using toxic (diethyl ether -DEE and chlorobenzene -CB) or nontoxic anti-solvents (ethyl acetate -AE) on the HP films formation. (ii) *Anti-solvent engineering of double perovskites*. We explored the effect of anti-solvents (CB, Tol and IPA) on the fabrication of 3D-3D ($K_{0.1}FA_{0.7}MA_{0.2}PbI_{2.8}Cl_{0.2}/CsPbBr_3$) and 3D-2D ($K_{0.1}FA_{0.7}MA_{0.2}PbI_{2.8}Cl_{0.2}/CsPb_2Br_5$)

- Fabricate and characterize small and large area standard PSCs, with organic HTL in all the cases, of different ETLs and engineered HPs described above, with Au contacts of different size/configurations–Fig. 3. In total 640 small and large area PSCs were fabricated so far.

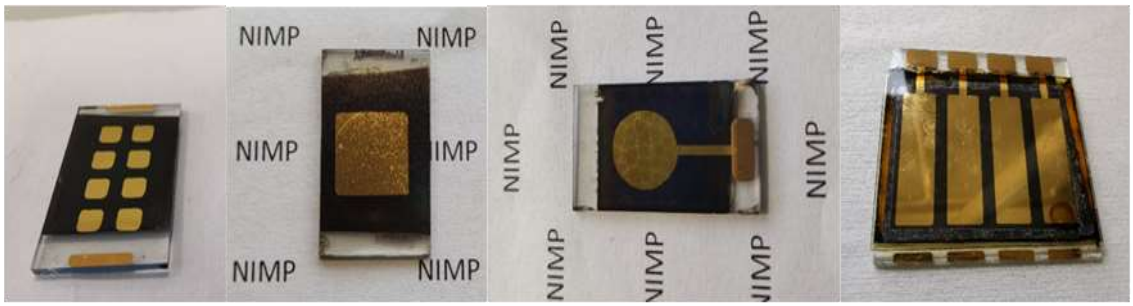

Figure 3: *Fabricated standard PSCs, different active areas, from 0.083 cm^2 to 2.4 cm^2.*

WP2: Preparation of inverted PSCs

PP (NIMP) had worked on:

- Deposition of HTL, HPs a and ETL, chemical and structural characterization As HTL, PEDOT:PSS films were deposited on ITO/glass and FTO/glass substrates. Three types of composition engineered HPs were deposited above the HTL: MAPbI2.6C0.4, (*MAPICl);* FA0.7K0.1MA0.2PbI2.6Cl0.4 (*FAMA10K)*; MAPbI1.8Br1.2 (*MAPIBr)*. As ETL, PCBM layers were deposited. To improve the PCBM properties, BCP (bathocuproine) was tested as an additive. The deposited films were investigated by XRD, AFM and SEM.
- Fabricate small area inverted PSCs, structural characterization

In total 824 of small area inverted PSCs, based on ITO/PEDOT:PSS and different compositions of HP and various dilutions of PCBM, were prepared and characterized by NIMP. Some photos are given in Fig. 4 with the corresponding SEM images in Fig. 5.

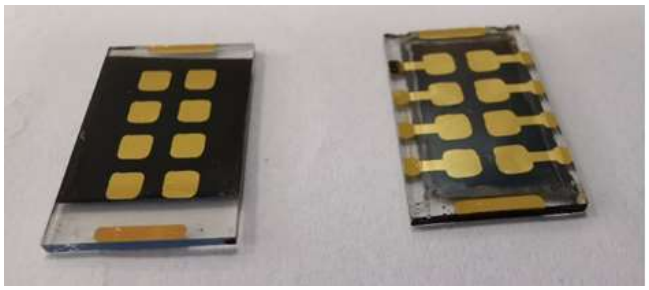

Figure 4. *Photos of electrode configurations in the fabricated small area inverted PSCs.*

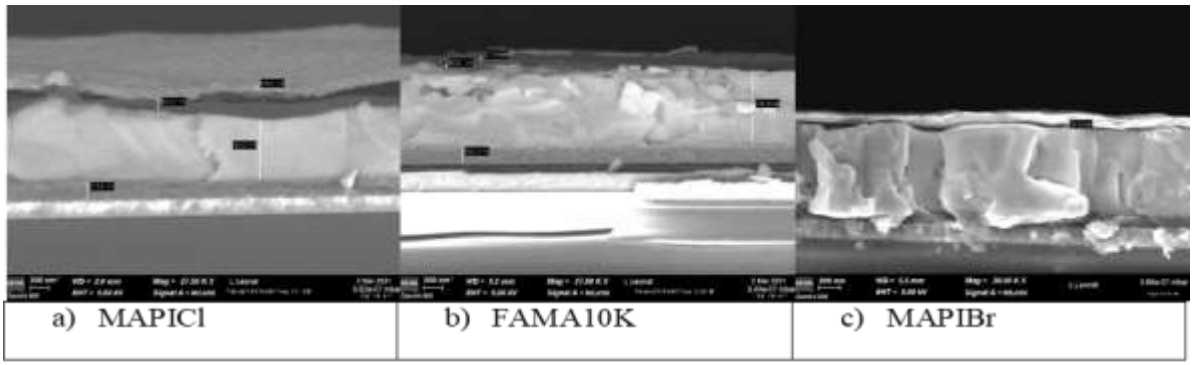

Figure 5*. SEM crossection images for inverted solar cells with three different perovskite compositions*

P1 (UiO) had worked on:

- Deposition of NiO_x films for HTMs in inverted PSCs. The films were RF sputtered on ITO coated glass and fused silica substrates. The deposition conditions were varied with respect to RF power, film thickness (10, 15 and 20 nm), temperature/annealing and O flow. The films were further characterized by optical transmittance (OT) and electrical conductivity. The main results are:

- A 1.58 W/cm^2 RF power results in 10 nm and 15 nm NiO_x films with good OT (Fig.6). The conductivity of NiO_x film is decreasing when the thickness is increased – see table 3.
- No significant change in OT is observed up to a deposition temperature of 200 ºC and post annealing in vacuum while. The OT and the bandgap are increasing with annealing in ambient atmosphere while are decreasing with the O flow (examples in Fig.7). OT and conductivity are inversely related.

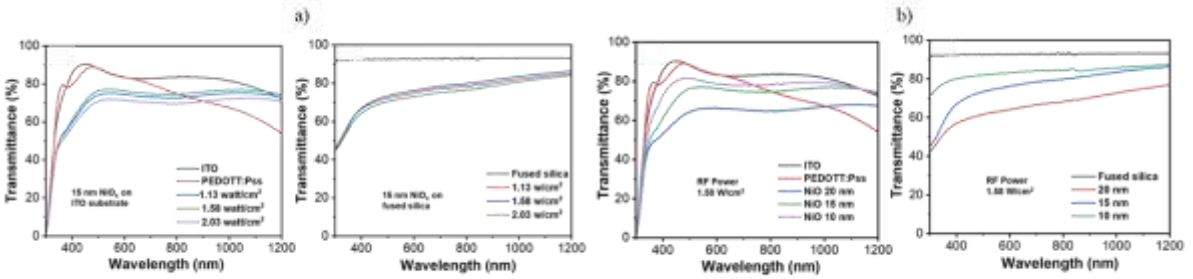

Figure 6. *Transmittance of: a) 15 nm NiO_x films at different RF power densities on bare ITO and on fused silica substrates (the PEDOT: PSS thin film on ITO substrate for comparison); b) NiOx films of different thickness on ITO and on fused silica substrates.*

Table 3: *Conductivity of NiO_x film for different thickness using four probes*

NiO Thickness	Current (nA)	Voltage (mV)	Sheet resistance (MΩ/Sq)	Conductivity (1/ Ω cm)
20 nm	100	24.49	1.02	4.5×10^{-1}
15 nm	10	23.32	9.72	7.4×10^{-2}
10 nm	10	69.39	28.94	3.1×10^{-2}

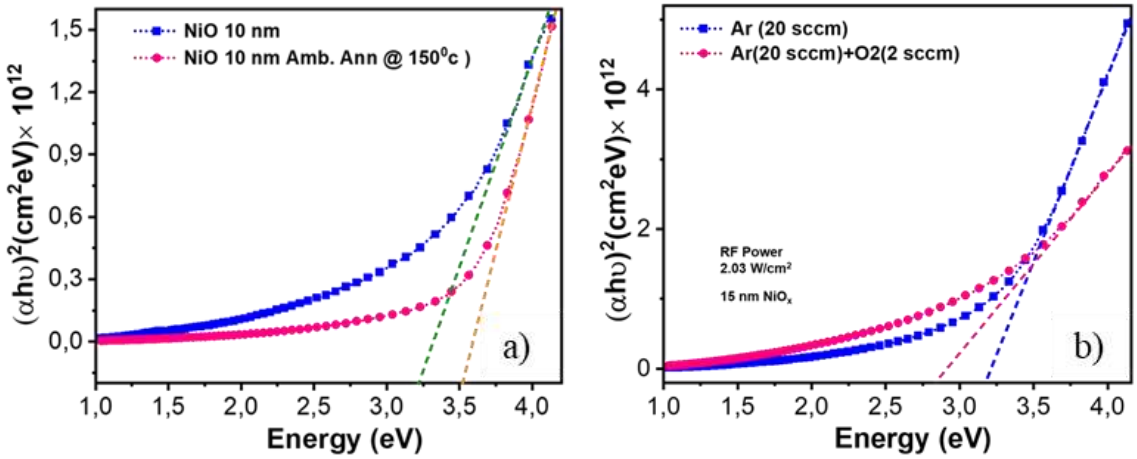

Figure 7. *Tauc plots for: a) 10 nm film, as deposited and ambient annealing; b) 15 nm film with and without oxygen flow.*

WP 3: Modelling of materials and interfaces

The theoretical work in 2021 was jointly performed by **P2(RU)** and **P3(NIPNE)** on: *Investigation of the electronic properties (band alignment) for MAPI – metal oxide interfaces*, based on ab initio density functional theory (DFT) calculations. Thus, the electronic properties of the interfaces between MAPI and several candidates for HTMs ETMs, relevant for PSCs, have been investigated. Specifically, we determined band alignment for the following interfaces: MAPI@Cu_2O, MAPI@NiO, MAPI@ $Cu_xNi_{1-x}O$ and MAPI@SnO_2. The influence of different types of point defects (vacancies, interstitials) was analyzed. We employed LDA+U correction in order to calibrate the band gaps as close as possible to the experimental values. Because NiO is anti-ferromagnetic, spin polarized calculations on a double supercell were performed in this case. The PDOS for each material and the band alignment at the interface with MAPI were determined – examples are given in Figures 8-10. We also calculate the changes in the band alignment due to all types of vacancies present in the studied interfaces (Cu, I, O, Ni, Pb, Sn).

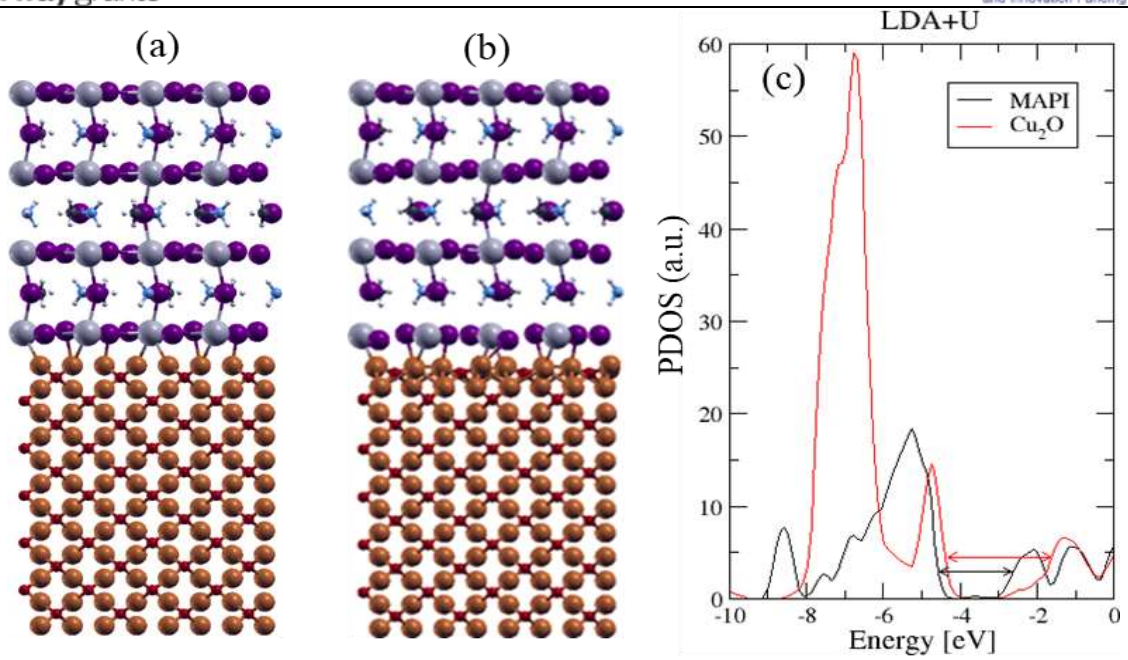

***Figure 8**: Ideal MAPI@CuO_2 interface: a) unrelaxed and b) relaxed atomistic depiction of the structure; c) Band alignment;*

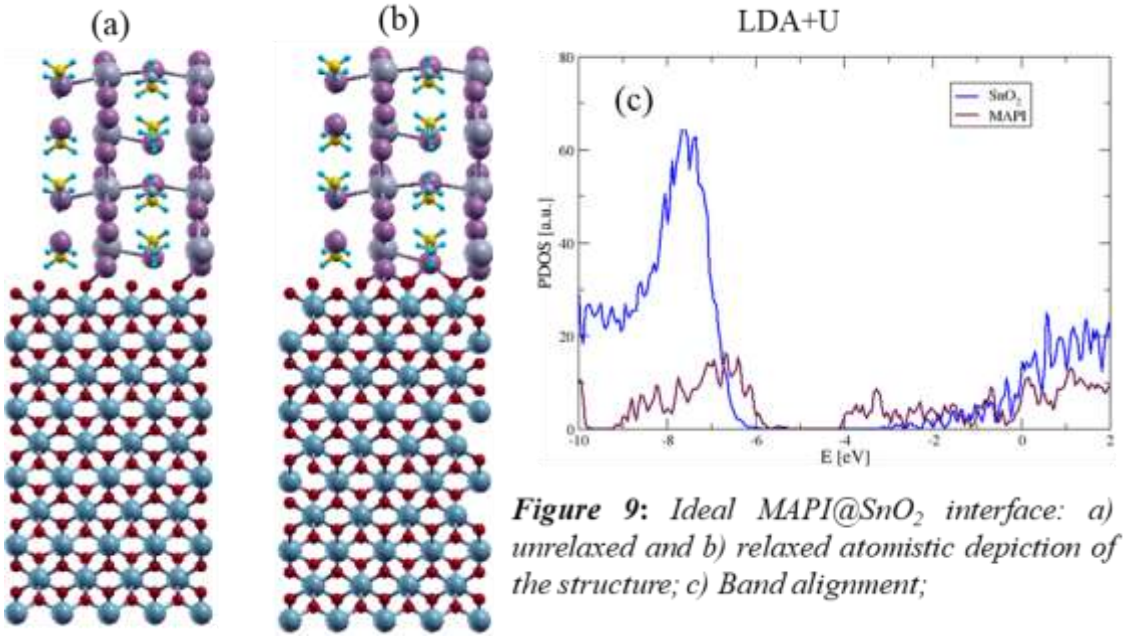

***Figure 9**: Ideal MAPI@SnO_2 interface: a) unrelaxed and b) relaxed atomistic depiction of the structure; c) Band alignment;*

The **P3(NIPNE)** team optimized the bulk oxide materials (Cu_2O, NiO, SnO_2) and performed initial DFT calculations on pristine and defected interfaces. These calculations were further extended by the **P2(RU)** team, in particular for the analysis of vacancies effects in MAPI@Cu_2O interface.

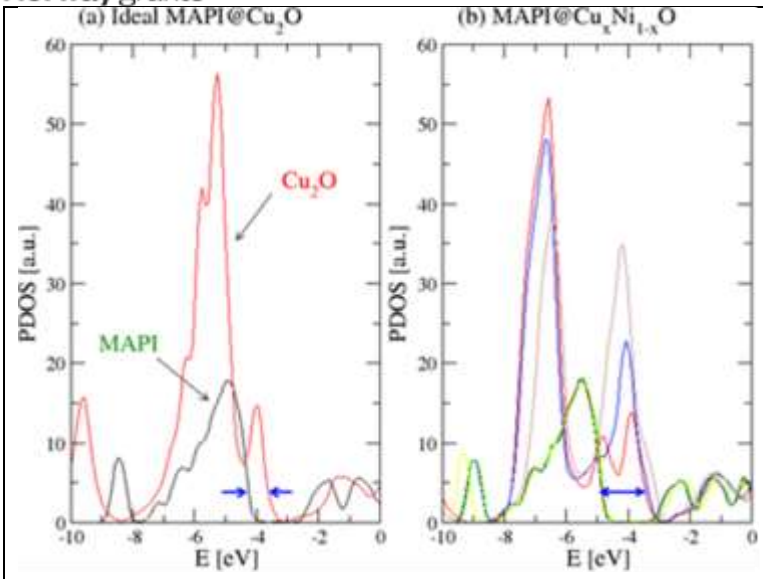

Figure 10: *Band alignment in ideal: (a) Cu_2O@MAPI interface; (b) MAPI@$Cu_xNi_{1-x}O$ interface (three different disorder realizations are shown). A larger valance band offset is obtained (marked by blue arrows).*

<u>WP4: Device characterization and modelling</u>

PP (NIMP) had worked on:

- *<u>Perform photovoltaic measurements on standard and inverted PSC devices, follow and analyze the stability of the photovoltaic performance in time</u>*

All the PSCs fabricated and characterized in WP1 and WP2 were measured to evaluate their photovoltaic performance. Examples of J-V curves obtained on standard (S) and inverted (I) PSCs are given in Fig. 11. All the characteristics were evaluated for extracting the R_{sh} and R_s, hysteresis index and PCE. Representative PSCs for different ETLs, HPs and HTMs were also monitored in time after fabrication to follow the degradation. An accelerated degradation takes place for HPs based on FAMA, which however slows down when FAMA is deposited on mesoporous QD-SnO_2.

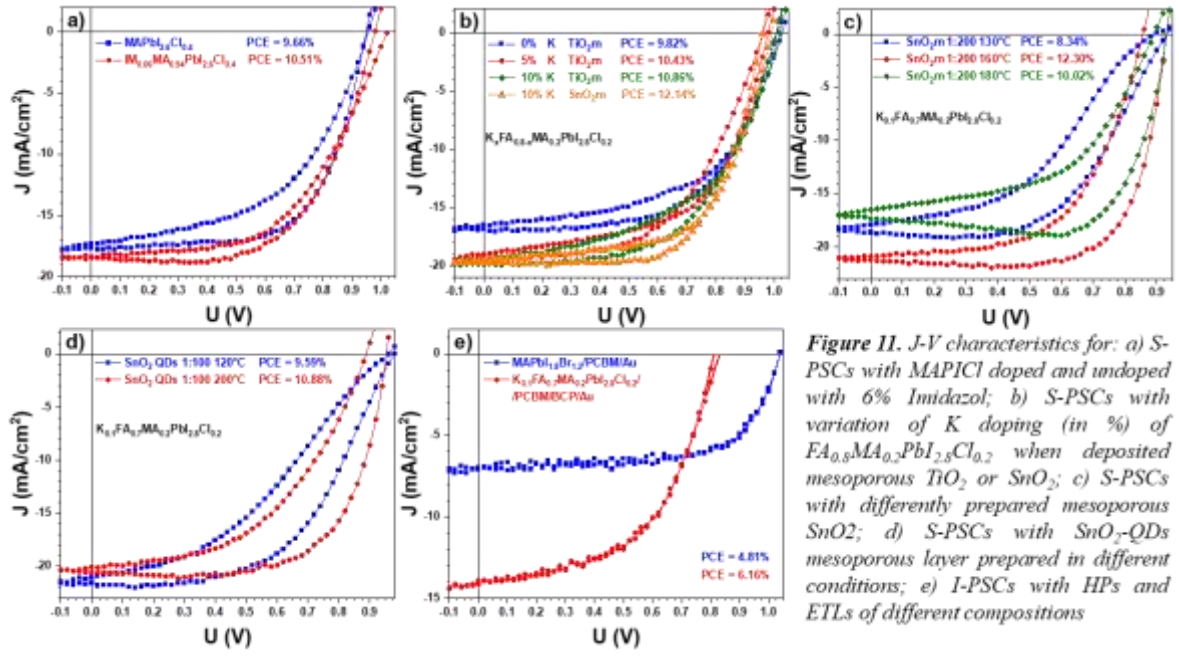

Figure 11. *J-V characteristics for: a) S-PSCs with MAPICl doped and undoped with 6% Imidazol; b) S-PSCs with variation of K doping (in %) of $FA_{0.8}MA_{0.2}PbI_{2.8}Cl_{0.2}$ when deposited mesoporous TiO_2 or SnO_2; c) S-PSCs with differently prepared mesoporous SnO2; d) S-PSCs with SnO_2-QDs mesoporous layer prepared in different conditions; e) I-PSCs with HPs and ETLs of different compositions*

- *<u>Perform impedance spectroscopy measurements and analyses</u>* of small and large signals for an experimental characterization of capacitive and inductive effects in S-PSCs in the presence or absence of light (1 SUN) and/or bias.

P3 (NIPNE) in partnership with P2(RU) worked on developing the models for large and small signal analysis and performed the numerical implementation*:*

- *The dynamical electrical model reproducing capacitive and inductive effects*

The previously proposed DEM model describing the capacitive effects was further developed to explain also the peculiar inductive phenomena. The proposed charge collection (CC) model (see Fig. 12a) is based on a new Ansatz for the recombination current (J_{rec}) and explains both, the apparent inductance and the large capacitance, providing the link to a microscopic description of these effects.

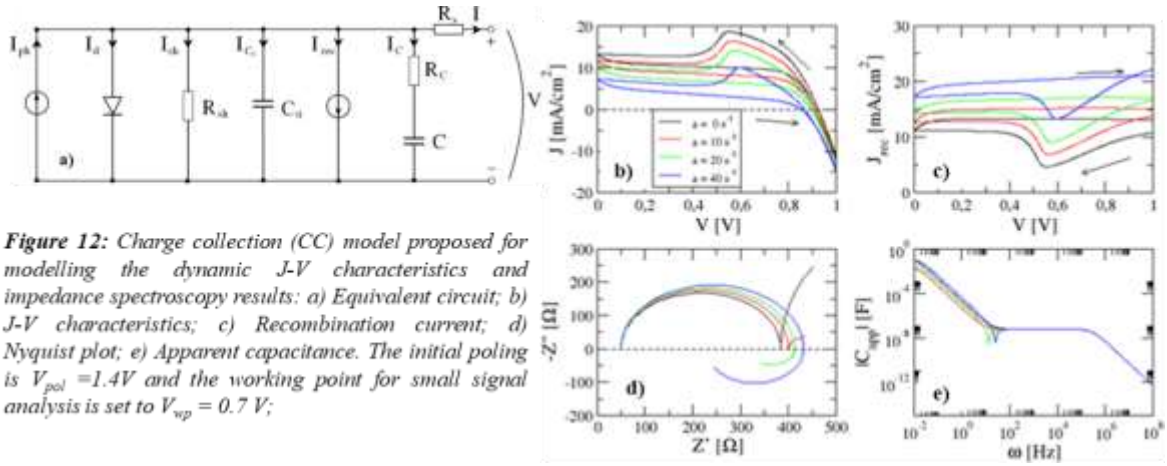

Figure 12: *Charge collection (CC) model proposed for modelling the dynamic J-V characteristics and impedance spectroscopy results: a) Equivalent circuit; b) J-V characteristics; c) Recombination current; d) Nyquist plot; e) Apparent capacitance. The initial poling is V_{pol} =1.4V and the working point for small signal analysis is set to V_{wp} = 0.7 V;*

Thus, the recombination current is modeled as $J_{rec} = J_{rec0} + a \cdot Q_c + b \cdot dQ_c/dt$. It includes the base recombination (J_{rec0}) and two terms, corresponding to inductive ($J_{rec,a} \sim Q_c$) and capacitive ($J_{rec,b} \sim dQ_c/dt$) effects. The *a* and *b* parameters tune the magnitude of the inductive and capacitive effects and are related to recombination effects, due to the ionic charge (Q_c) and ionic current (dQ_c/dt). We explored the effects in J-V characteristics and small signal analysis, by changing the inductive component of J_{rec}, through $a = 0, 10, 20, 40\ s^{-1}$, while $b=10^3$ is constant (Fig. 12b). As J_{rec} increases with *a,* the inductive effects become visible in Nyquist plots. The hysteretic phenomena, caused by ionic migration, can be correlated with the apparent huge capacitance and inductive effects.

WP5: Device encapsulation and modules production and testing in standard operation conditions

PP(NIMP) had worked on:

- *fabrication and characterization of small and large area standard PSCs*
- *evaluate the degradation effects* in as –fabricated and encapsulated PSCs

P4(WATTROM) had worked on:

- *elaborate the encapsulation procedure for* the PSCs produced by PP
- *perform the encapsulation and design the degradation tests*

The encapsulation process steps with EVA/PET foils are exemplified in Fig.13 for a large area standard PSC based on FAMA type of HP. The PSCs were tested under various humidity conditions, while the V_{oc} was simultaneously recorded. The non-encapsulated cell kept its initial V_{oc} only up to 40% humidity in air where the total degradation of the cell occurred (Fig. 14). The encapsulated cell showed a good resistance up to 90% humidity with only a small decrease in V_{oc}.

Encapsulation steps

1. The PSC was covered with EVA foil. In order to assure the EVA bonding on PSC surface, the cell was placed for 30 seconds on a hot-plate fixed at 80 °C.
2. The PET foil was added on top of EVA foil, while keeping the cell at 80 °C. The PET foil was lightly pressed with a glass slide for 30 seconds at 80 °C.

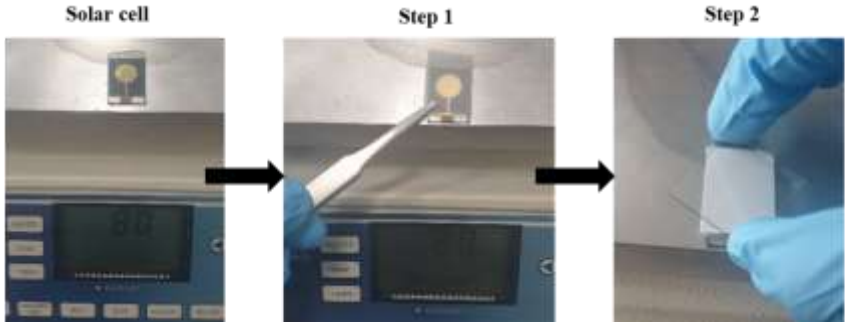

Figure 13: shows the photocurrent measured under 1 SUN illumination, before and after encapsulation at 80 °C with EVA/PET foils. No signs of degradation was observed after the proposed encapsulation process.

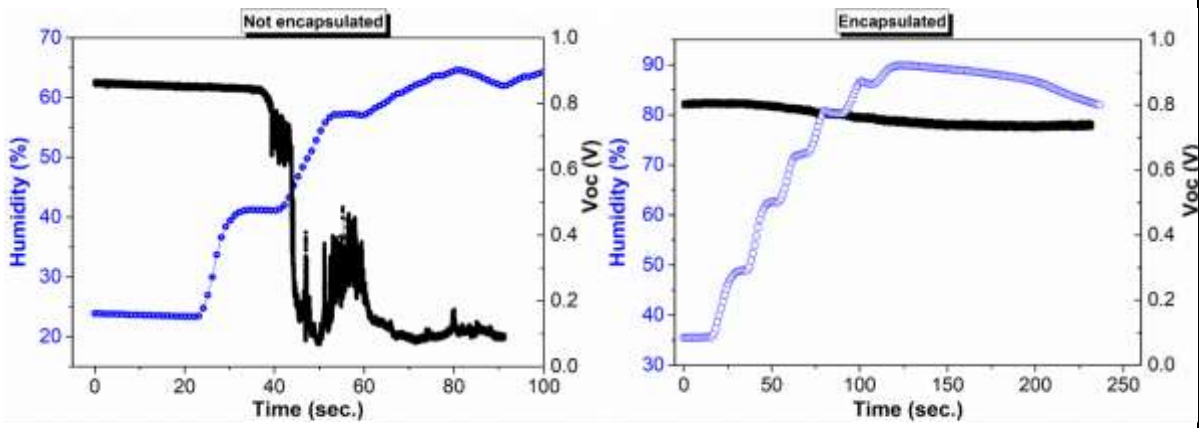

Figure 14. *Voc evolution in time under increased air humidity for PSCs encapsulated or not.*

WP6: Management, reporting, dissemination and patenting

All the partners participate in managing their resources and disseminate the results. **PP(NIMP)** took care of the project management, project webpage and made the yearly report based on the specific contributions of the partners.

Overview of the progress of work towards the objectives of the project, including milestones (M) and deliverables (D) identified in the project contract.

The progress of the work performed in 2021 towards the project objectives was in accordance with the EEA36 contract, all the tasks starting in 2021 being addressed (see the first part of this report). The milestones (MS) and deliverables (D) in 2021 are presented below.

- ***MS1: Functional printing system:*** *Install the printing equipment in glow box*

A slot die system for deposition of organic and hybrid layers in PSCs was purchased in May 2021. For inorganic layers we have used an in-house developed and patented spray-coating machine. The new blade system was first tested in ambient atmosphere for establishing the working parameters for depositing PEDOT:PSS, PCBM and the halide perovskites (HPs) based on CH_3NH_3 (MA) and CH_5N_2 (FA) organic cations. Due to the requirements imposed by the difficult solubilization of PbI_2, only solvents with a high evaporation temperature, such as DMF and DMSO with boiling points at 153ºC and 189ºC, respectively, can be used for obtaining the proper crystalline phase. We succeed adjusting the deposition for all HP layers except the ones containing FA, which require a crystallization temperature where solvents

start to boil. A lower temperature leads to the formation of different crystalline phases, not suitable for solar cells - see Fig. 15 below for FAMA@10K perovskite. While for spin-coating of FA containing HPs, the crystallization temperature can be reduced to 130°C by adding few drops of a miscible solvent with a lower evaporation temperature, this trick is not compatible with the blade coating technique. However, the MA based HP films crystalize close to 110°C and can be successfully deposited with dr. Blade. The new system was installed in an in-house built glovebox in November 2021 (Fig. 15b).

Sample			
Temperature (^{0}C)	130	145	150

Figure 15. *a) Example of $FA_{0.7}K_{0.1}MA_{0.2}PbI_{2.6}Cl_{0.4}$ (FAMA@10K) thin films deposited by dr. Blade at different substrate temperatures; b) Slot die printing system installed in in-house made glowbox*

- ***D1 - Project webpage*** - http://perla-pv.ro , available from june 2021

- ***D2 - Report-optimization of printed TiO_2, SnO_2 ETMs,*** *presented below.*

We used the spray coating as printing method suitable for large area deposition of ETMs in PSCs. Optimization studies concerning dilution, temperature and annealing time lead to the deposition of an optimized 60 nm compact TiO_2 (c-TiO_2) layer for both ITO and FTO coated glass substrates. Due to the smallest roughness of ITO films, the c-TiO_2 layer was also more homogeneous and used further for depositing mesoporous (m) TiO_2, SnO_2 and Quantum Dots of SnO_2 (QD-SnO_2).

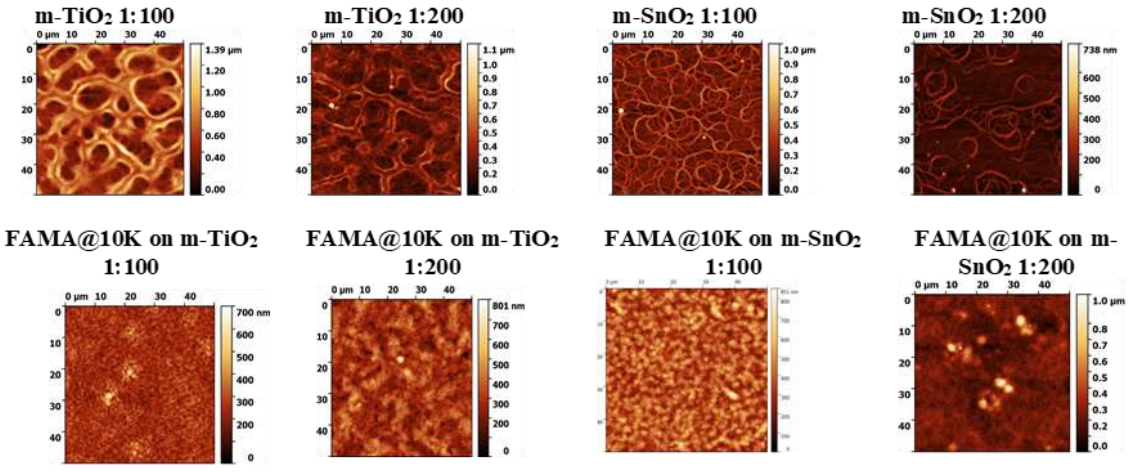

Figure 16. *AFM images of the mesoporous layers (upper) deposited all at 120°C and of the perovskite films deposited on the mesoporous layers (down)*

While for the deposition of m-TiO_2 and m-SnO_2 we used commercial suspensions, the QDs-SnO_2 suspension was prepared in-house. The printing technology was optimized by varying the suspensions dilution, deposition temperatures. In total, 108 samples were prepared and characterized by XRD, AFM and SEM. The dilution was varied from 1:100 to 1:400 and the deposition temperatures from 100 to 200°C. The HP films are compact and pinholes free. The HP layer is uniform when deposited on m-TiO_2 with a dilution of 1:100 (see Fig.16) and the RMS values are increasing with solvent ratio. For m-SnO_2, the RMS values of the HPs are lower than when deposited on m-TiO_2.

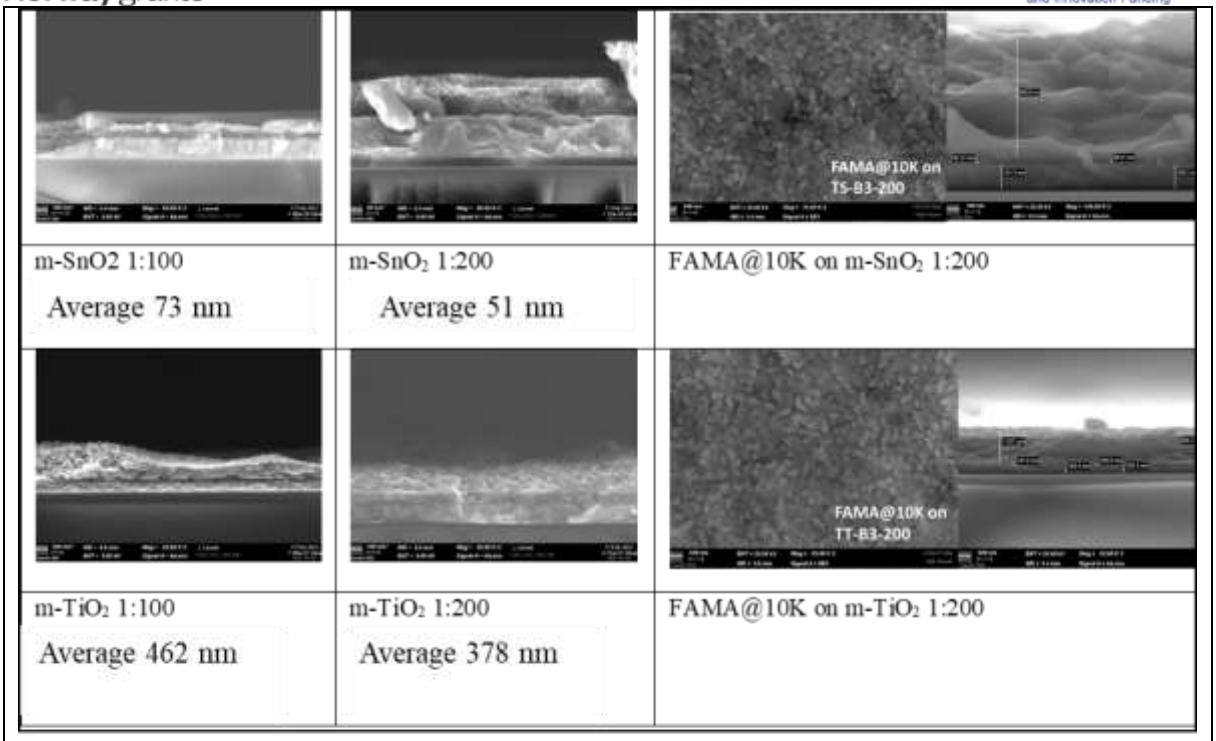

***Figure 17**. SEM images of the mesoporous layers and of the FAMA@10K perovskite films deposited on TiO_2 and SnO_2 mesoporous layers with 1:200 dilutions.*

SEM images (Fig. 17) revealed that the average thickness of the m-layers decreases with increasing the solvent ratio. The XRD on FAMA@10K layer revealed that when is deposited on m-TiO_2, the crystallite size is increasing with increasing dilution (from 90 to 100 nm) while, when is deposited on m-SnO_2 it decreases (from 86 to 60 nm).

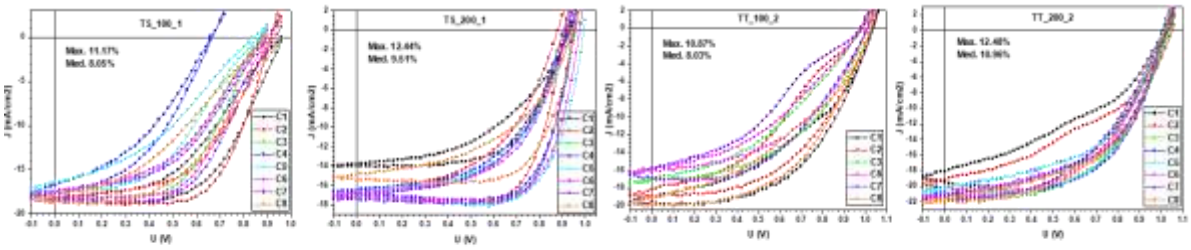

***Figure 18**. Photovoltaic measurements for the solar devices prepared on compact TiO_2 with m-TiO_2 (TT) and m-SnO_2 (TS) with 1:100 and 1:200 dilutions.*

A number of 48 PSC samples (ITO/c-TiO_2/m-TiO_2 or m-SnO_2/FAMA@10K/Spiro-OMeTAD/Au), each with 8 gold contacts, were prepared by varying the dilutions used for the deposition of the mesoporous layers at 120°C (where the m-TiO_2 was found to have the best performance). According to the photovoltaic measurements (Fig. 18), the 1:200 dilutions for m-TiO_2 and m-SnO_2 deliver the best performance in the investigated PSCs. The maximum achieved PCEs are 12.48 % and 12.44 % for cells with m-TiO_2 1:200 (noted TT_200) and m-SnO_2 1:200 (labelled as TS_200), respectively. As for FA containing HPs the use of m-SnO_2 is the most promising ETL, further experiments focused on this material by varying the deposition temperature from 120 to 200°C. The AFM images of the FAMA@10K deposited on c-TiO_2/m-SnO_2 showed that all the films are compact and smooth, irrespective of SnO_2 solution and deposition temperature (Fig. 19) except for those deposited at 130°C from commercial solution, exhibiting rough surface (RMS=300 nm) and large voids.

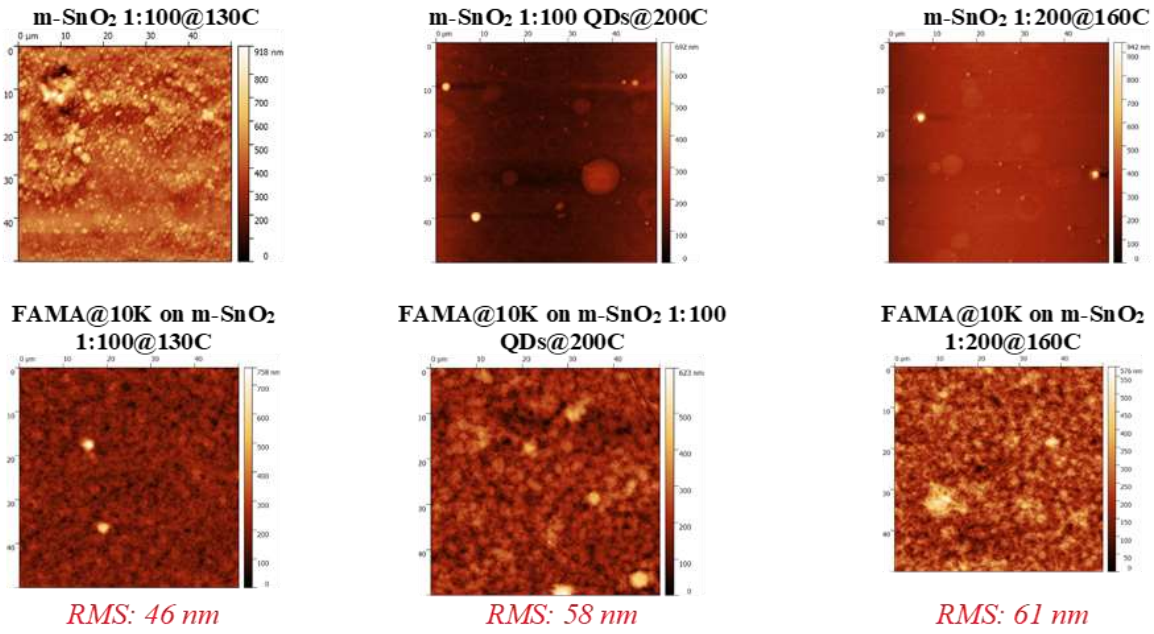

***Figure 19**. AFM images of the mesoporous SnO_2 and QD-SnO_2 layers deposited at different temperatures and of FAMA@10K films deposited above.*

Photovoltaic measurements show that temperatures larger than 120 ^oC leads to an increase of the PCE in the corresponding PSCs with SnO_2 based mesoporous ETLs (Fig. 20).

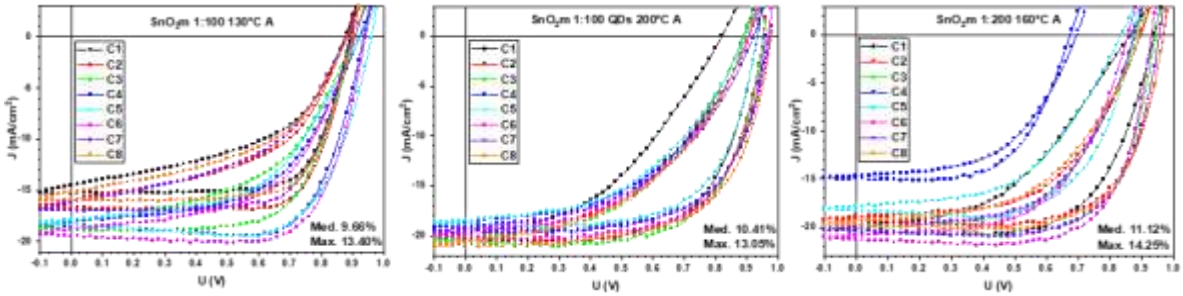

***Figure 20**. Photovoltaic measurements for the solar devices prepared with m-SnO_2 deposited at different temperatures.*

The optimal conditions for printing the mesoporous ETLs in FA based PSCs, are: (i) 120^oC and a 1:200 dilution for m-TiO_2 ; (ii) 160^oC and a 1:200 dilution when SnO_2 commercial suspension is used, and 200^oC and a 1:100 dilution when QDs-SnO_2 solution is used.
Further studies to complete the optimization process of ETLs (month 24 of the project) will continue including also other HPs.

- ***D3 - First year report –*** *delivered in February 2022*

- ***D4 - Modelling the defect states and charge accumulation at interfaces-*** *presented below*

We investigated the electronic properties of the interfaces between MAPI and several candidates for HTMs and one ETM, relevant for PSCs. Specifically, we determined band alignment for the interfaces of MAPI with SnO_2, Cu_2O, $Cu_xNi_{1-x}O$ and NiO. The atomic structure and the electronic properties of the bulk oxides were calculated considering the LDA+U correction needed to calibrate the band gap of materials as close as possible to

experimental values (examples given above for the description of work done in WP3, Figs. 8-10). Point defects may alter the band alignment, which, depending on their type can be beneficial or detrimental for the role of oxides used as ETM or HTM. We calculated the changes in the band alignment due to defects naturally occurring at these interfaces (vacancies and interstitials). These changes are shown in Fig. 21-23.

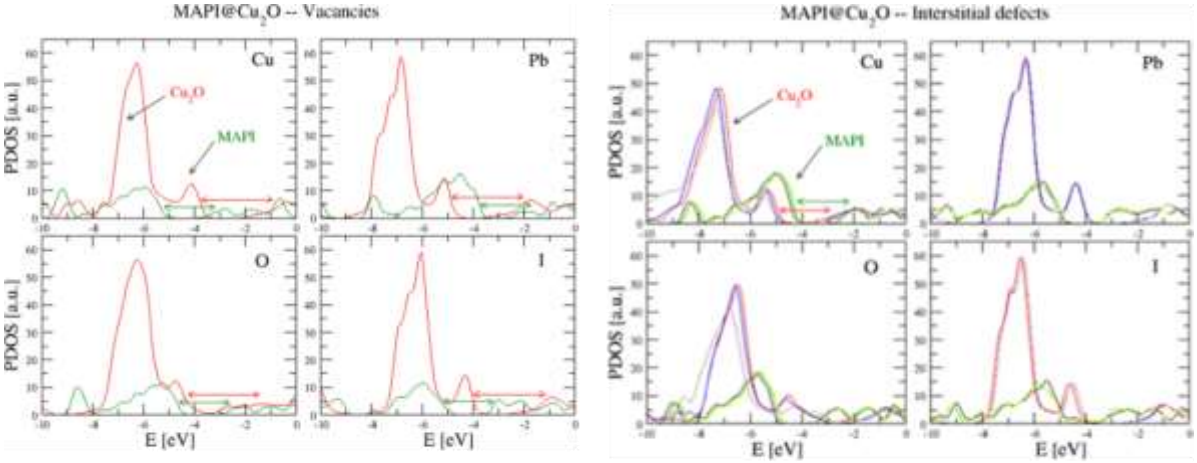

Figure 21: *Band alignment in MAPI@Cu_2O interface in the presence of vacancies and interstitials.*

For Cu_2O and NiO, used as HTM in contact with MAPI, Cu, Ni and I vacancies enhance the valence band offset while the presence of O and Pb vacancies reduce or even revert the band alignment (Pb vacancies in MAPI/Cu_2O case).

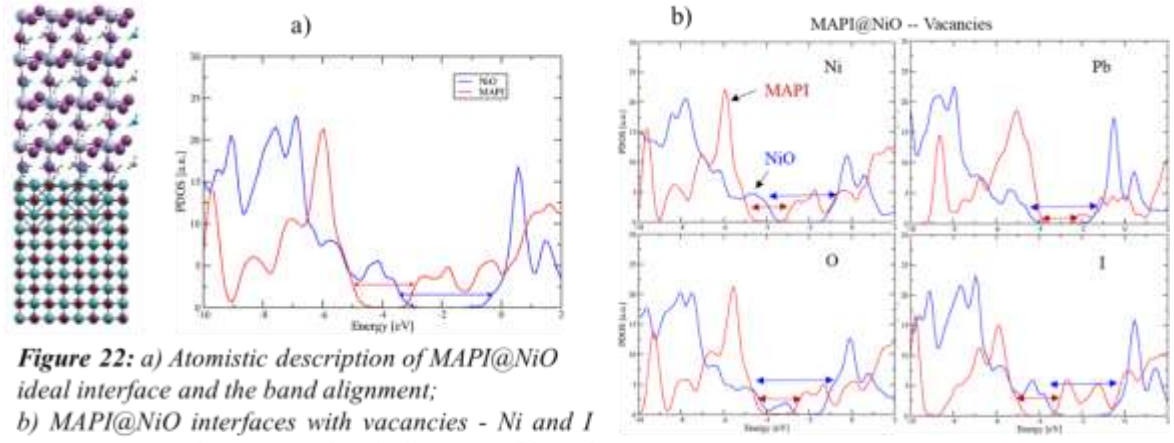

Figure 22: *a) Atomistic description of MAPI@NiO ideal interface and the band alignment;*
b) MAPI@NiO interfaces with vacancies - Ni and I vacancies provide a proper band alignment; Pb and O vacancies are detrimental.

The role of SnO_2 as ETM for a MAPI@SnO_2 interface is not clearly evidenced for pristine materials. However, some vacancies can favour a proper band alignment. Thus, our calculations showed that Pb and O vacancies provide a proper band alignment, while Sn and I vacancies not.

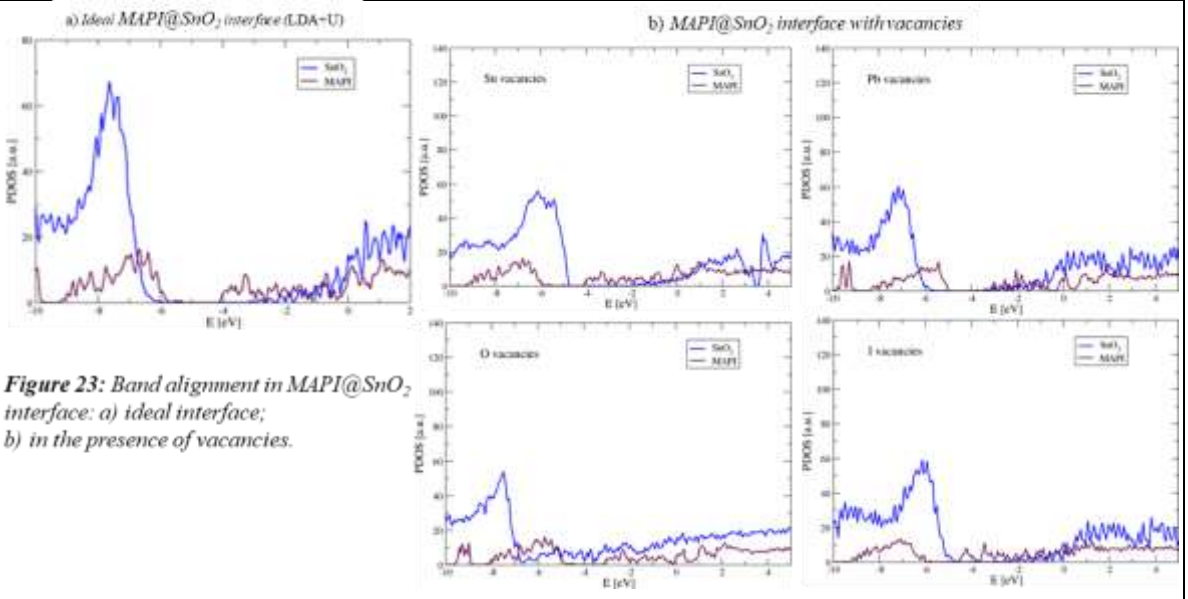

Figure 23: *Band alignment in MAPI@SnO_2 interface: a) ideal interface; b) in the presence of vacancies.*

The presence of defect states and charge accumulation at the interfaces result in peculiar capacitive and inductive effects revealed by impedance spectroscopy and dynamic J-V characteristics of PSCs. For explaining such effects, two types of dynamic electrical models were developed so far, of charge accumulation (CAM) and of drift-diffusion (DDM). While the CA models are easy to use by experimentalists, they assume unphysical large charge accumulations and meaningless inductive elements (L) - see Fig. 24a. In contrast, the DDM offer good physical descriptions of both, capacitive and inductive effects, but the calculations are very complex to be currently employed for simulating experimental data. Therefore, we developed an easy to be applied model, called further the charge collection model (CCM).

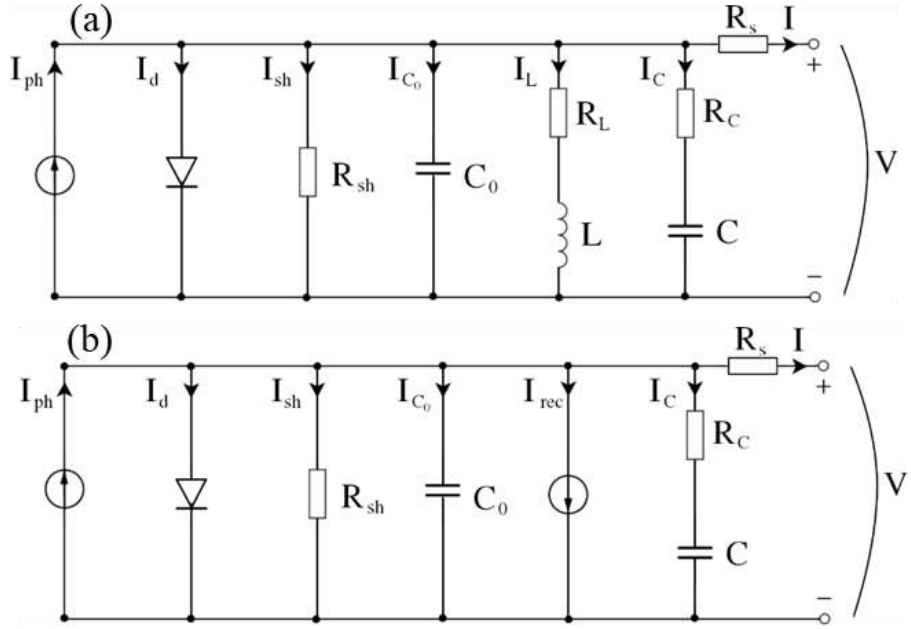

Figure 24: *Equivalent circuit models: (a) Charge accumulation (polarization) (CAM); (b) Charge collection (CCM).*

The CCM is accounting for defect states and charge accumulations at the interfaces and describes the experimentally observed capacitive and inductive effects in PSCs. The small signal equivalent circuit is depicted in Fig. 24b. The CCM considers that the recombination current (I_{rec}) is controlled by the ionic current, proportional with the electric field (E_{Field}) in the perovskite ($I_{ion} = \mu_{ion} E_{Field}$). The presence of I_{ion} causes hysteresis in J-V characteristics. The band diagrams for two bias prepoling conditions (V_{pol}), followed by reverse scans starting from V_{oc}, for normal (NH) or inverted (IH) hysteresis are depicted in Fig. 25.

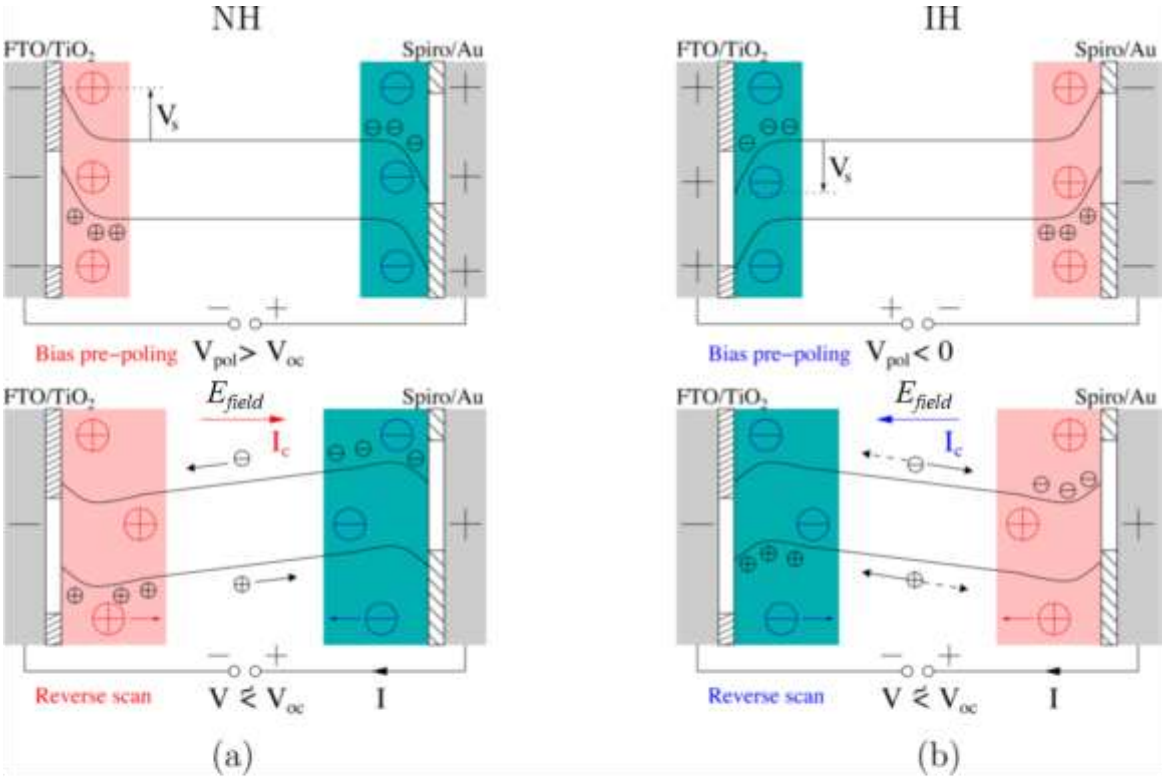

***Figure 25**. Schematics of band diagrams corresponding to prepoled samples, followed by reverse scans starting from Voc. The bias prepoling condition V_{pol} determines the appearance of NH or IH: (a) Vpol > Voc (NH) and (b) Vpol < 0 (IH). During the measurement the interfacial charge is displaced, generating the current Ic. The hashed regions represent the conduction and valence bands of the ETL and HTM layers. The dashed arrows mark the movement direction of the carriers once the normal operation condition is recovered.*

Thus, as E_{Field} modulates the ionic distribution, it also modulates the recombination rate in the HP. It results that the apparent inductance and the large measured capacitances, are effects due to particular forms of J_{rec}. The density of the recombination current is modeled in CCM as: $J_{rec} = J_{rec0} + a \cdot Q_c + b \cdot dQ_c/dt$, which includes the base recombination (J_{rec0}) and two terms, one accounting for the ionic charge interfaces ($J_{rec,a} \sim Q_c$) inducing inductive effects and another proportional to the ionic current ($J_{rec,b} \sim dQ_c/dt$) responsible for the capacitive effects. The *a* and *b* parameters tune the magnitude of the inductive and capacitive effects. We explored these effects in the J-V characteristics and small signal analysis, by changing the inductive component of J_{rec}, through the *a* paramater ($a = 0, 10, 20, 40\ s^{-1}$), while $b=10^3$ remains constant. As shown in Fig. 26 (a,b) J_{rec} increases with *a*. As the inductance component grows larger it becomes visible in Nyquist plots, where Z'=Re[Z] and Z"=Im[Z]. The apparent capacitance $C_{app}(\omega) = \omega^{-1}\mathrm{Im}[Z^{-1}]$ grows to very high values, while the ionic capacitance C is still 1000 times smaller (Fig. 26d).

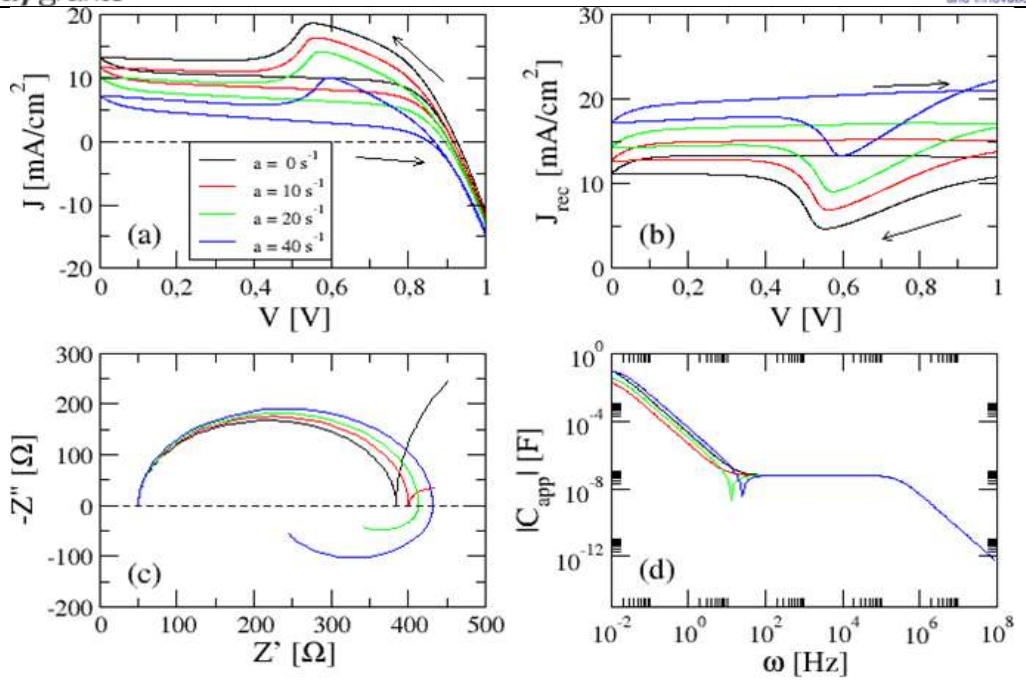

Figure 26: *Dynamic J-V characteristics and impedance spectroscopy: a) J-V characteristics; b) Recombination current; c) Nyquist plot; d) Apparent capacitance. The initial poling is V_{pol} =1.4V and the working point for small signal analysis is set to V_{wp}=0.7 V;*

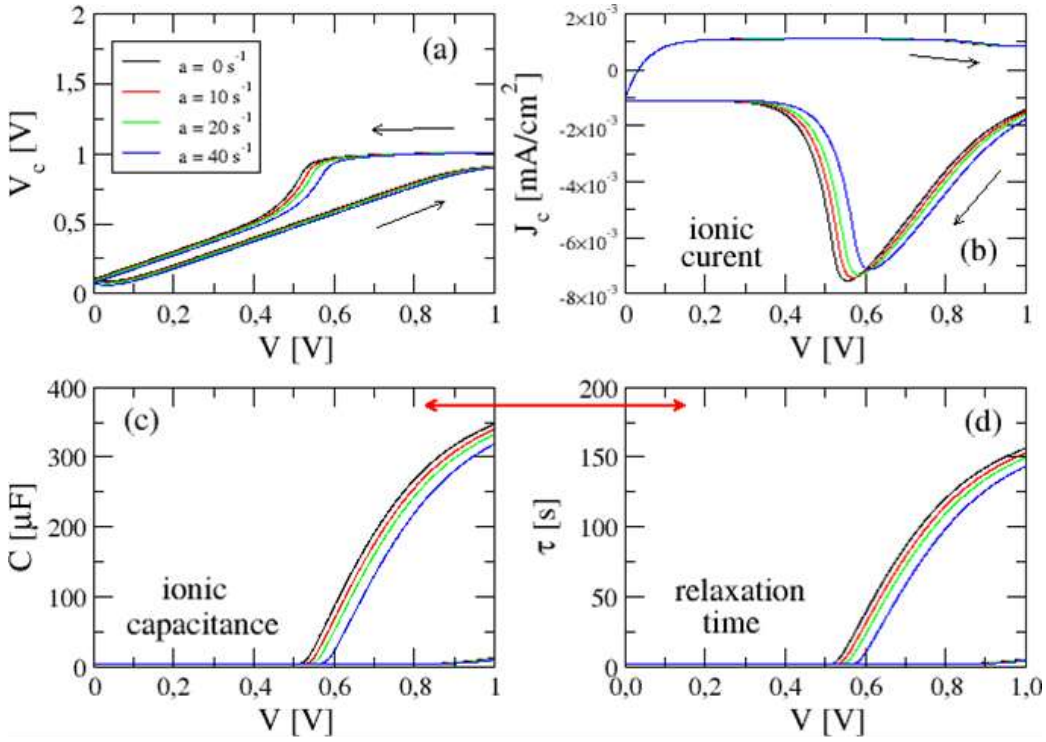

Figure 27: *a) Voltage on the ionic capacitor V_c(V); b) Ionic current J_c(V); c) Ionic capacitance C(V); d) Relaxation time τ(V).*

Fig. 27 shows further details concerning: voltage on non-linear ionic capacitor (V_c), density of the ionic current (J_c) and dependence on the external voltage of ionic capacitance C(V) and instant relaxation time τ(V). Increasing the *a* parameter, J_{rec} increases while C(V) and τ are lowered. Based on the proposed CC model we show that the ionic migration, responsible for the hysteretic phenomena, controls the recombination current in the device and this way it can be directly correlated with the apparent huge capacitance and inductive effects. Applied on different devices, subjected to different measurement and atmospheric conditions, the model brings potential for optimization of PSCs by identifying the physical processes responsible for the degradation.

- ***D18 – 2 ISI publications in 2021 (from 9 foreseen over the 3 years project duration)***

Details on the exploitation and dissemination of the results and of the activities

The project activities and results obtained in 2021 were disseminated in the scientific community by the presented contributions during participation in international conferences as well as via the published articles in scientific ISI quoted journals.

Scientific abstracts and summary of the activities employed in PERLA-PV project are also accessible from the webpage of the project (http://perla-pv.ro/).

Conferences:

C1) Electronic and stability properties of alkyl-based two-dimensional halide perovskites, G.A. Nemnes, N. Filipoiu, T. L. Mitran, S. Derbali, F. Neatu, A. G. Tomulescu, C. Besleaga, A. Mirea, S. Neatu, I. Vlaicu, M. Florea, I. Pintilie, EMRS2021 Fall Meeting, 20-23 September 2021 - oral presentation on 22nd of September 2021, section: Materials for Energy, see https://www.european-mrs.com/materials-energy-applications-hydrogen-storageproduction-solar-cells-super-capacitors-thermoelectr-0

C2) Dynamic J-V Hysteresis in Perovskite Solar Cells: Measurement Protocols and Physical Interpretations, I. Pintilie et al, IUMRS-ICA 2021, 3-8 October 2021, Jeju, Korea – invited talk 4th October, section Energy Materials and Devices, see *http://www.iumrs-ica2021.org/download/program/[01]MoB1.pdf*

Articles:

A1) Tetragonal–Cubic Phase Transition and Low-Field Dielectric Properties of $CH_3NH_3PbI_3$ Crystals, R.E. Patru, H. Khassaf, I. Pasuk, M. Botea, MihaelaL. Trupina, C.P. Ganea, L. Pintilie, Lucian, I. Pintilie***, Materials*** *2021,14(15), 4215;* *https://doi.org/10.3390/ma14154215*

A2) Enhancing stability of hybrid perovskite solar cells by imidazolium incorporation, A.G. Tomulescu, L. N. Leonat, F. Neațu, V. Stancu, V. Toma, S. Derbali, Ș. Neațu, A. M. Rostas, C. Besleagă, R. Pătru, I. Pintilie, M. Florea, Solar Energy Materials & Solar Cells 227 (2021) 111096; https://doi.org/10.1016/j.solmat.2021.111096

Towards perovskite large area photovoltaics

Project code:	EEA-RO-NO-2018-0106 (SEE-36)
Project acronym:	PERLA-PV
Duration:	01.01.2021 – 31.12.2023
Total budget from the Programm (euro):	1,164,000
- Grant (85%):	989.400
- Co-financing (15%):	174.600
Own budget (euro):	545.530
Project Webpage:	http://perla-pv.ro/
Project Promoter organization:	INCDFM
Principal Investigator:	Ioana Pintilie
Project Partner organization (1):	Universitatea Oslo
Project Partner organization (2):	Universitatea Reykjavik
Project Partner organization (3):	IFIN-HH
Project Partner organization (4):	WATTROM -Tritech Group SRL

The EEA Grants represent the contribution of Iceland, Liechtenstein and Norway towards a green, competitive and inclusive Europe.

There are two overall objectives: reduction of economic and social disparities in Europe, and to strengthen bilateral relations between the donor countries and 15 EU countries in Central and Southern Europe and the Baltics.

The three donor countries cooperate closely with the EU through the Agreement on the European Economic Area (EEA). The donors have provided €3.3 billion through consecutive grant schemes between 1994 and 2014. For the period 2014-2021, the EEA Grants amount to €1.55 billion. The priorities for this period are: 1) Innovation, Research, Education and Competitiveness; 2) Social Inclusion, Youth Employment and Poverty Reduction; 3) Environment, Energy, Climate Change and Low Carbon Economy; 4) Culture, Civil Society, Good Governance and Fundamental Rights; 5) Justice and Home Affairs